JOURNAL OF AIRCRAFT
Vol. 33, No. 2, March–April 1996

Review of Forebody-Induced Wing Rock

L. E. Ericsson,* M. R. Mendenhall,† and S. C. Perkins Jr.‡
Nielsen Engineering and Research, Inc., Mountain View, California 94040

Wing rock at moderate angles of attack is often generated by dynamic wing stall; however, the wing rock of most concern is generated by the vortices shed from the aircraft forebody at high angles of attack. The capability to understand and predict forebody-induced wing rock is a prerequisite for the successful design of agile aircraft and missiles that are required to perform maneuvers at high angles of attack. Available information on the wing rock experienced by advanced aircraft is reviewed and an explanation of the flow physics causing the wing rock is presented.

Nomenclature

b = wingspan
d = local body diameter
k = proportionality coefficient, Fig. 13
l = rolling moment, coefficient $C_l = l/(\rho_\infty U_\infty^2/2)Sb$
l' = sectional lift, coefficient $C_l = l'/(\rho_\infty U_\infty^2/2)d$
p = roll rate
Re = Reynolds number, $U_\infty d/\nu_\infty$
S = reference area, projected wing area
t = time
U = velocity
α = angle of attack
Δ = increment or amplitude
$\Delta\theta$ = crossflow separation offset from the lateral meridian
Λ = wing leading-edge sweep
ν = kinematic viscosity
ρ = fluid density
Φ = body roll angle
φ = body azimuth, Fig. 9

Subscripts
W = wall
0 = initial conditions
∞ = freestream conditions

Differential symbol
$\dot{\phi}$ = $\partial\phi/\partial t$

Introduction

A REVIEW of experimental results for advanced aircraft operating at high angles of attack reveals that they usually experience wing rock of one kind or another.[1] For aircraft with straight or moderately swept wings, wing rock occurs first at moderate angles of attack. This type of wing rock is generated by the negative damping-in-plunge of the wing sections caused by dynamic airfoil stall.[2] If the aircraft has a long, slender nose, which often is the case, forebody vortices will generate wing rock at higher angles of attack where the wings are fully stalled. This type of wing rock has been documented in experiments with a generic aircraft model.[3] The flow mechanism driving the wing rock is in this case the downwash on the wing generated by the forebody vortices.[4,5] The X-29A aircraft experiences this type of forebody-induced wing rock.[6,7] When the inner portion of the wing has a highly swept leading edge, as in the cases of the F-18 HARV and X-31 aircraft, the high-alpha wing rock is generated by direct interaction between the forebody vortices and the leading-edge vortices from the inboard wing panels.[8]

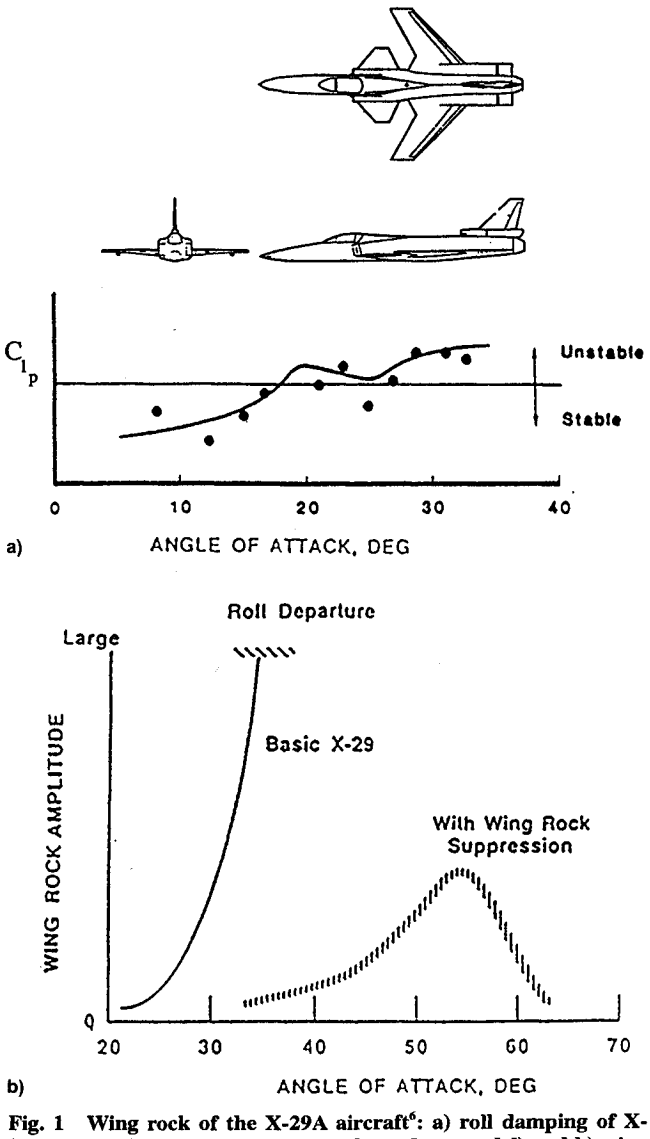

Fig. 1 Wing rock of the X-29A aircraft[6]: a) roll damping of X-29A models (—— = wind tunnel and • = drop model) and b) wing rock characteristics of the X-29A aircraft.

Presented as Paper 94-0167 at the AIAA 32nd Aerospace Sciences Meeting and Exhibit, Reno, NV, Jan. 10–13, 1994; received Dec. 10, 1994; revision received Aug. 14, 1995; accepted for publication Aug. 18, 1995. Copyright © 1995 by the authors. Published by the American Institute of Aeronautics and Astronautics, Inc., with permission.

*Consulting Engineer. Fellow AIAA.
†Vice President. Associate Fellow AIAA.
‡Research Engineer. Member AIAA.

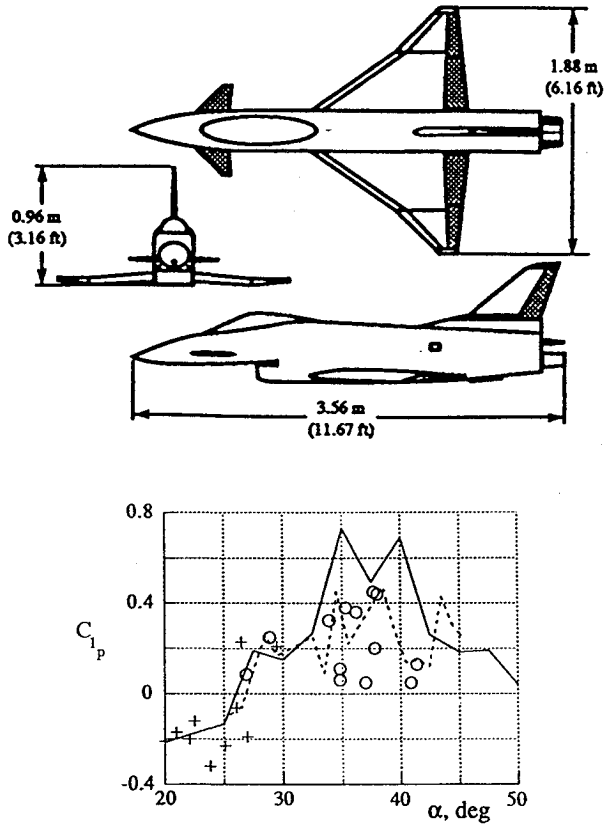

Fig. 2 Roll damping of the X-31 aircraft.[9] Drop model: ○ = single maneuvers, ---- = partitioned data, —— = wind tunnel, and + = full-scale aircraft.

The experimental results[6] in Fig. 1 for the X-29 aircraft show the high-alpha trends discussed previously. Wing rock occurs first at moderate angles of attack, caused by a loss of roll damping through dynamic wing stall[1,2] at $\alpha > 18$ deg (Fig. 1a). When this wing rock was suppressed by the use of the ailerons, forebody-induced wing rock[4,5] occurred at $\alpha > 30$ deg (Fig. 1b). The measured roll damping of the X-31 aircraft[9] (Fig. 2) indicates similar high-alpha data trends. At $\alpha > 25$ deg the moderately swept outer wing panels may generate wing rock through the dynamic stall process,[1,2] but at $\alpha > 30$ deg the wing rock is more likely to be of the forebody-induced type.[8] The F-18 HARV aircraft exhibits similar wing rock characteristics[10] (Fig. 3), with the forebody-induced variety starting at $\alpha > 35$ deg.

A landing aerospace plane could experience forebody-induced wing rock as demonstrated by the results[11] in Fig. 4. In the absence of the fuselage, the 78-deg delta wing experiences slender wing rock.[12] When the slender nose of the fuselage was substituted by a hemispherical nose, no wing rock occurred,[13] as expected, because no forebody vortices exist in the tested α range.[14] On the slightly blunted six-caliber ogive forebody of the actual fuselage, forebody vortex shedding should start at $\alpha > 20$ deg,[14] producing the wing rock observed in the experiment (Fig. 4).

The purpose of this article is to review previous work describing the flow physics behind the forebody-induced wing rock phenomenon.

Discussion

Moving wall effects[15] contribute to wing rock through their influence on the forebody crossflow separation and associated vortex shedding.[4,5,8] They are very dependent upon the crossflow Reynolds number with regard to the nature of their induced aerodynamic effects, as illustrated by Magnus lift measurements on a rotating circular cylinder[15,16] (Fig. 5). For laminar flow conditions, positive Magnus lift is generated, mainly as the result of the separation delay on the top side through the downstream moving wall effects. In contrast, at critical flow conditions, negative Magnus lift is generated by the promotion of transition on the bottom side through up-

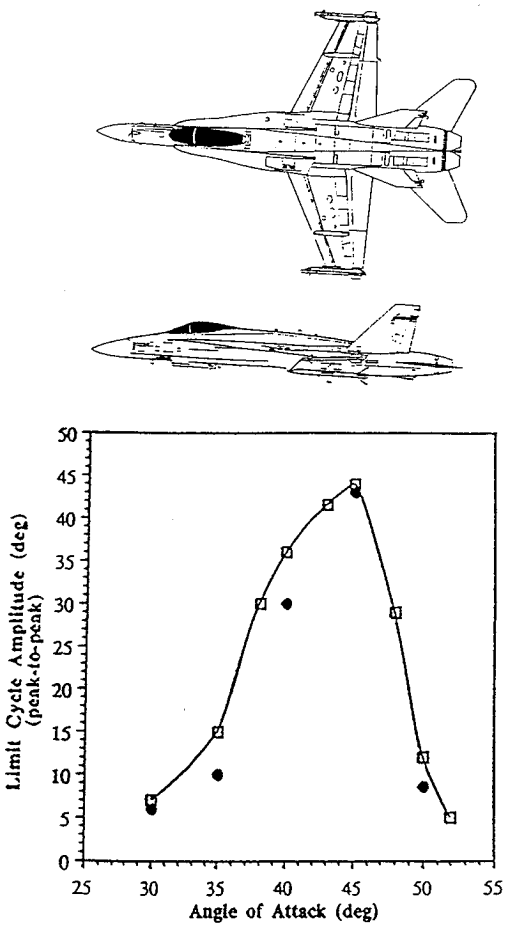

Fig. 3 Wing rock of the F-18 HARV aircraft.[10] □ = wind-tunnel data and ● = HARV flight data.

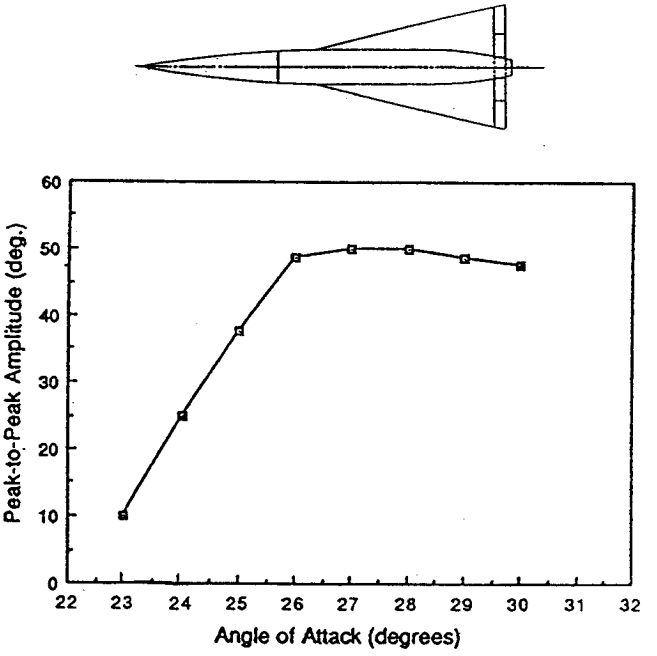

Fig. 4 Wing rock of slender delta wing body.[11]

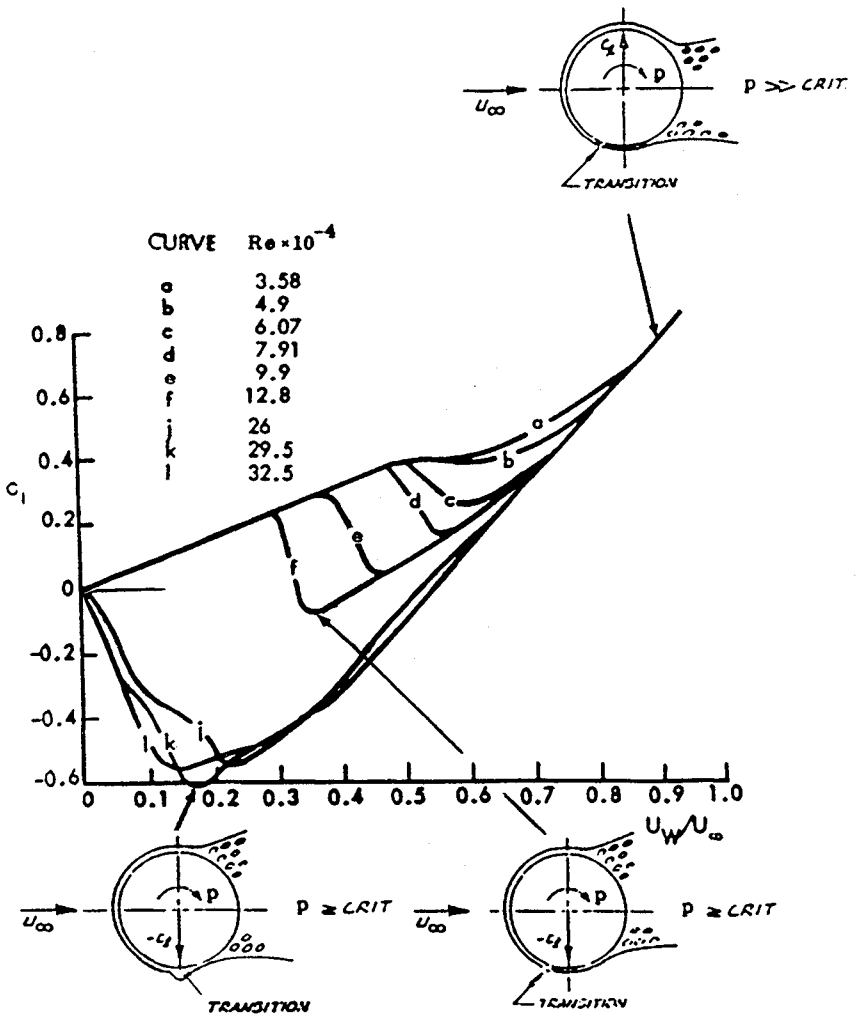

Fig. 5 Magnus lift of rotating circular cylinder.[16]

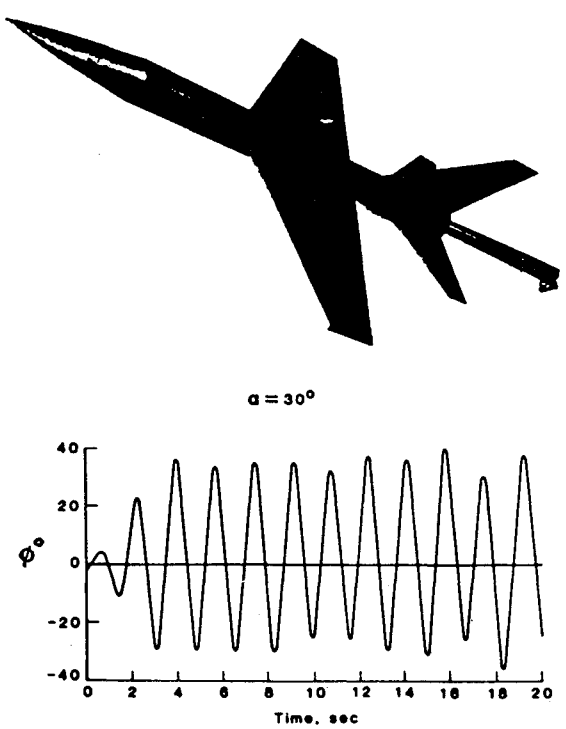

Fig. 6 Wing rock of generic aircraft configuration.[3]

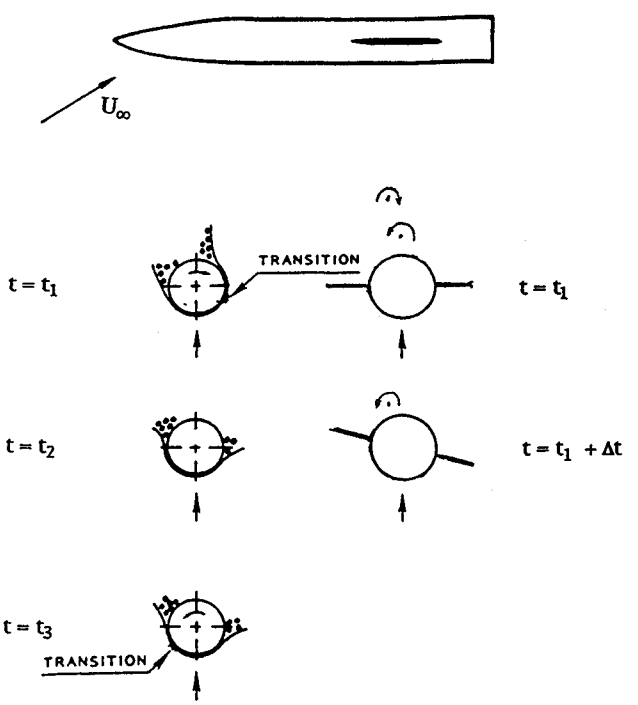

Fig. 7 Conceptual flow mechanism for forebody-induced wing rock.[4]

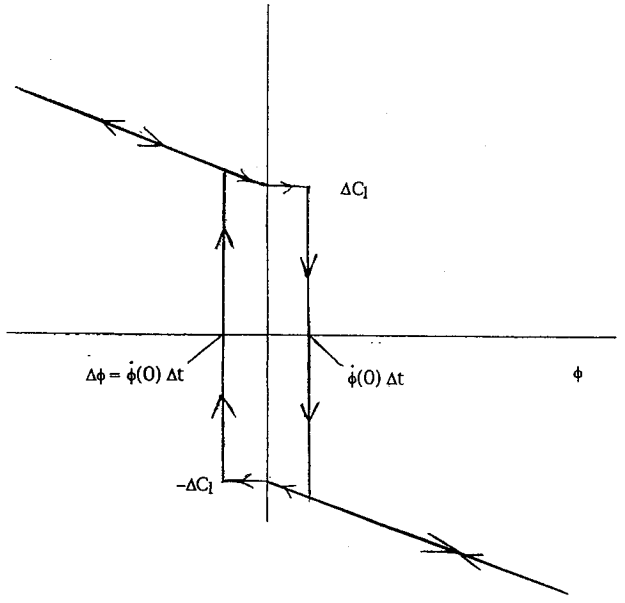

Fig. 8 Conceptual time-lag-induced undamping hysteresis.

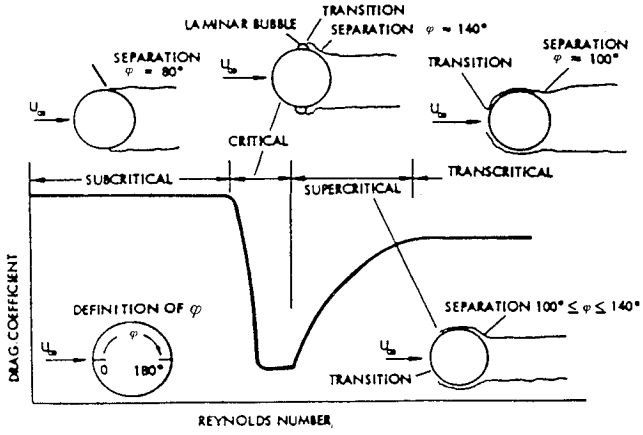

Fig. 9 Circular cylinder crossflow drag.[18]

stream moving wall effects, causing a change from the subcritical to the supercritical type of flow separation, e.g., at $Re = 0.128 \times 10^6$ and $U_W/U_\infty \geq 0.3$ (curve *f* in Fig. 5). The negative Magnus lift reaches its maximum magnitude when the initial, static crossflow conditions are of the critical type (curves *j*, *k*, and *l* in Fig. 5).

In the analysis in Refs. 4 and 5 of the experimentally observed wing rock of a generic aircraft[3] (Fig. 6), it was assumed that critical crossflow conditions existed on the forebody. The Reynolds number based upon the diameter of the cylindrical aft body was $Re = 0.26 \times 10^6$; i.e., in the critical *Re* regime[16] (Fig. 5). Thus, the crossflow over the nose and nose shoulder will be in the critical region. The scenario in Fig. 7, envisioned in Refs. 4 and 5, is summarized here. At $t = t_1$, the adverse upstream moving wall effect on the forebody crossflow causes boundary-layer transition to occur earlier, as illustrated in the figure. The effect is similar to that of changing the separation from the subcritical to the supercritical type in Fig. 5. In the absence of time-lag effects, the vortex geometry sketched at

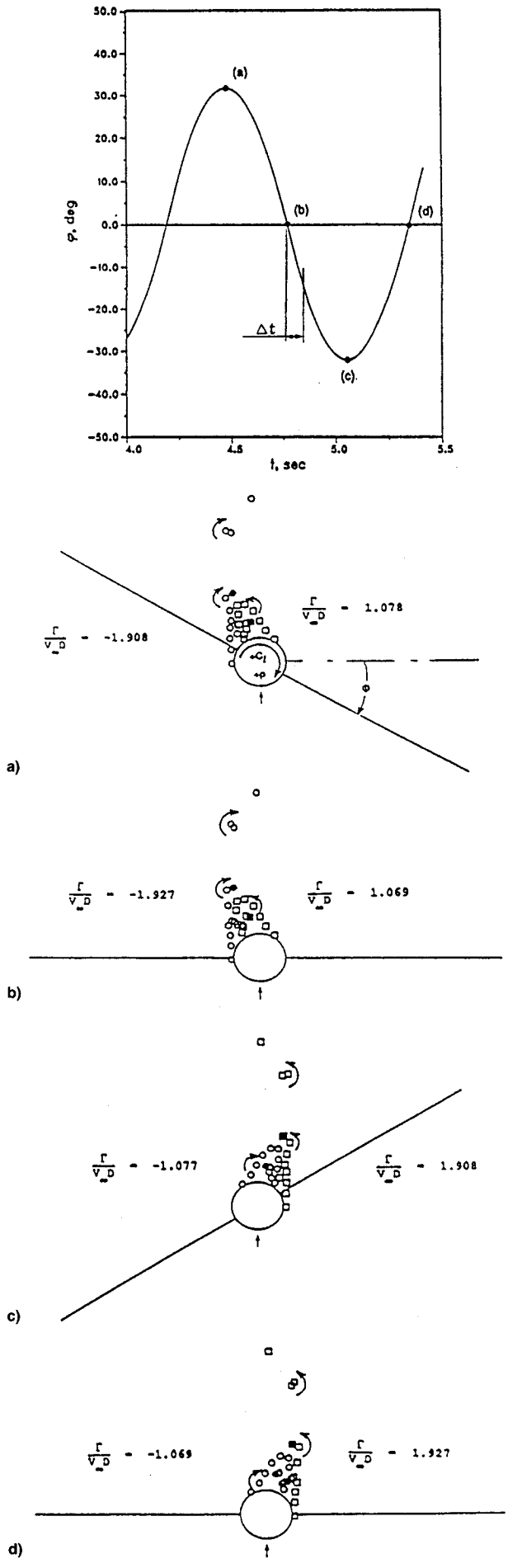

Fig. 10 Computed wing rock time history.[17] $\alpha = 35$ deg, $\phi_0 = 20$ deg, and $\Delta\theta = 40$ deg. a) $t = 4.47617$ s, $\phi = 31.77016$ deg, $p = -0.53$ deg/s, $C_l = -0.037$; b) $t = 4.76837$ s, $\phi = 0.19751$ deg, $p = -194.37$ deg/s, $C_l = -0.019$; c) $t = 5.05435$ s, $\phi = -32.02274$, $p = 0.55$ deg/s, $C_l = 0.037$; and d) $t = 5.34654$ s, $\phi = -0.14465$, $p = 195.53$ deg/s, $C_l = 0.019$.

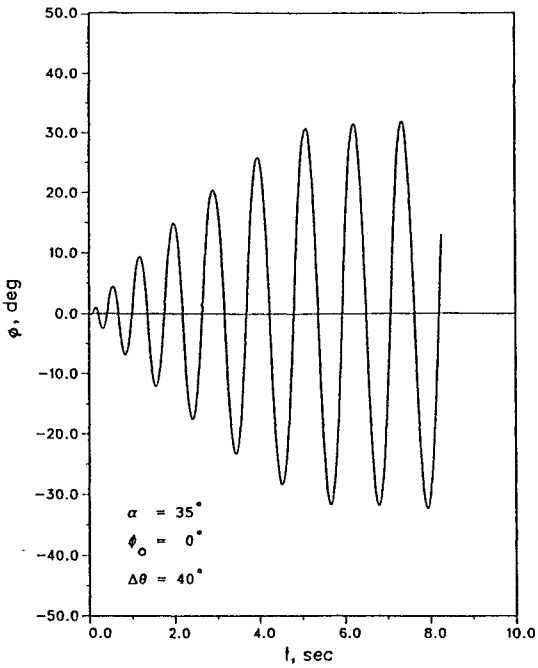

Fig. 11 Computed wing rock amplitude.[17]

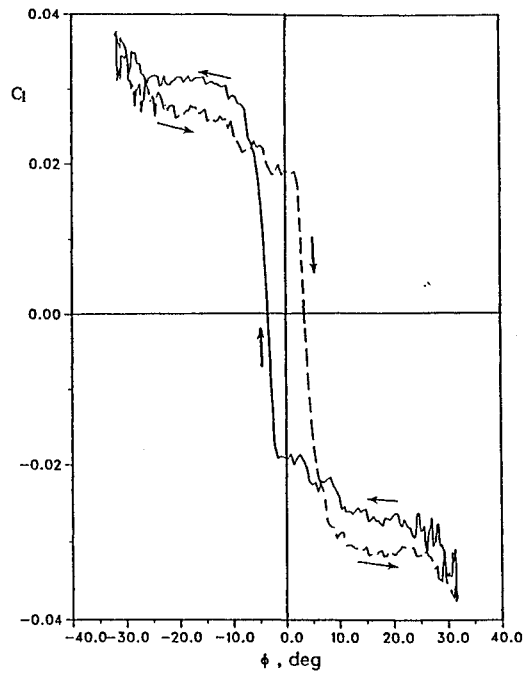

Fig. 12 Computed $C_l(\phi)$ loop.[17]

$t = t_1$ would result. Because of time-lag effects similar to those for slender wing rock,[12] this vortex geometry is not realized until $t = t_2 = t_1 + \Delta t$. For simplicity, only the vortex closest to the body is shown at t_2, as it indicates the direction of the vortex-induced rolling moment.

At $t = t_3$, when the roll rate reaches its maximum in the opposite direction, another forebody switch of flow separation asymmetry occurs. Because of the time lag effect, the vortex geometry influencing the now horizontal wing has not changed, but is the same as at $t_2 = t_1 + \Delta t$, in agreement with the flow visualization results in Ref. 3. During the time lag Δt, the vortex-induced rolling moment drives the rolling motion, generating the observed wing rock.[3] This is illustrated in Fig. 8. The rolling moment increment ΔC_l, induced by the switch of forebody flow separation and vortex asymmetry, is statically stabilizing. The roll angle $\dot{\phi}\Delta t$, generated by the time lag Δt, makes ΔC_l have a dynamically destabilizing effect.

In Ref. 17, the type of discontinuous characteristics around $\phi = 0$ shown in Fig. 8 were included in an analytic method for prediction of the wing rock characteristics of the generic aircraft model for the axisymmetric nose and without the tail surfaces present. The results of that investigation are summarized here. Based upon experimental results for a circular cylinder[18] (Fig. 9), it was assumed that laminar flow separation occurred at the lateral meridian on one side, whereas on the other side, critical flow separation was delayed to 40 deg past the lateral meridian; due to the adverse upstream moving wall effect on transition, discussed earlier in conjunction with Fig. 5. It was further assumed that the favorable, downstream moving wall effect delays laminar flow separation to occur at 90 deg rather than 80-deg latitude.

Figure 10 shows the results of the computation described in Ref. 17 for $\alpha = 35$ deg, $\phi_0 = 20$ deg, and $\Delta\theta = 40$ deg. The vortex cloud generated by the forebody[19] is shown at the wing leading edge for four different roll angles, $\phi \approx 30$ deg, $\phi = 0$, $\phi \approx -30$ deg, and $\phi = 0$ (a, b, c, and d, respectively, in Fig. 10). It can be seen that at Fig. 10a a restoring rolling moment $C_l = -0.037$ is generated, which drives the oscillation back towards $\phi = 0$. At Fig. 10b, when $\phi = 0$ is reached, the negative rolling moment generated by the forebody vortices at a time increment Δt earlier, $C_l = -0.019$, still exists, driving the roll oscillation. Not until the time increment Δt later, at $\phi < 0$, does the new forebody-induced vortex cloud reach the wing, starting to add to the restoring rolling moment, which reaches $C_l = 0.037$ at Fig. 10c. When $\phi = 0$ is reached again, the positive rolling moment generated by the forebody vortices, $C_l = 0.019$, continues to drive the wing rock. In free flight the limit cycle oscillation results when the driving rolling moment is balanced by the roll damping generated by the fully stalled wing. In Ref. 17 a value was assumed for the roll damping that included the effect of the bearing friction present in the test.[3]

Figure 11 shows that the computed amplitude time-history[17] is in qualitative agreement with the experimentally observed wing rock characteristics[3] (Fig. 6), and Fig. 12 shows that the computed undamping $C_l(\phi)$ loop for $|\phi| < 10$ deg has many of the characteristics sketched in Fig 8. The slanted up- and downstroke branches of the undamping, inner loops in Fig. 12, instead of the vertical ones in Fig. 8, could have resulted from the fact that individual vortices in the vortex cloud have slightly different time lags depending upon where on the forebody they originated, whereas the loop in Fig. 8 assumes the existence of a single time lag. The outer damping loops in Fig. 12 were obtained by applying the roll damping needed to provide the limit-cycle oscillation observed in the test.[3,20] In free flight, somewhat similar damping loops are produced by the deep-stall damping-in-plunge of the wing sections.

The predicted amplitude buildup (Fig. 11) is much slower than that observed in the experiment[3] (Fig. 6). This is true even when allowing for the fact that the amplitude buildup is significantly faster for the elliptic cross-sectional body[21] (Fig. 6) than for the analyzed circular cross section[17] (Fig. 11). It is pointed out in Ref. 5 that the experimentally observed fast amplitude buildup is the likely result of a growth from half-cycle to half-cycle of the extent of the asymmetric flow separation, resulting in a $C_l(\phi)$ loop of the type sketched in Fig. 13. As the amplitude $|\phi|$ grows, the roll rate $|\dot{\phi}|$ grows, and with it the magnitude of the moving wall effect (Fig. 5). This results in a half-cycle to half-cycle growth of the wing-rock-driving $C_l(\phi)$ loop, through the cycle-to-cycle area increase $2k[\dot{\phi}(0)]^2\Delta t$ shown in Fig. 13.

The amplitude buildup for the 2.5% model of the F-18 HARV, observed in low-speed tests[10] at $\alpha = 40$ deg (Fig. 14), looks very similar to that shown in Fig. 11. Thus, one expects the aerodynamic characteristics to have some of the charac-

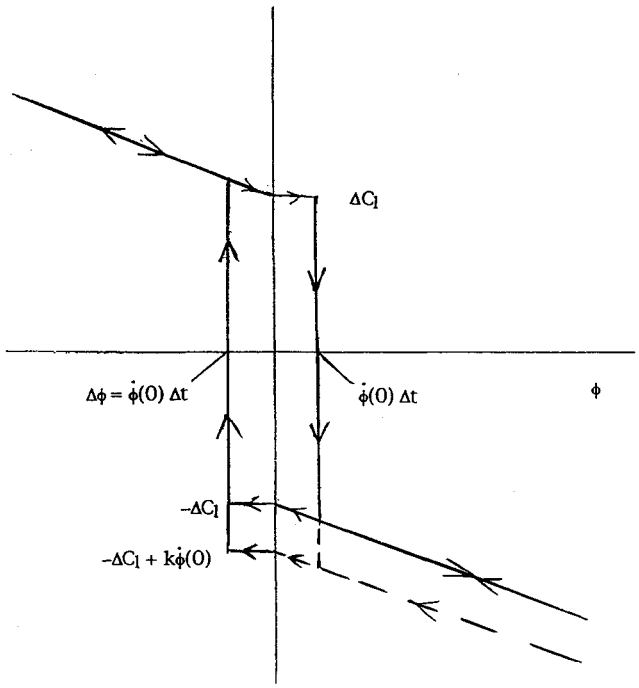

Fig. 13 Conceptual roll-rate-induced increase of the undamping hysteresis.

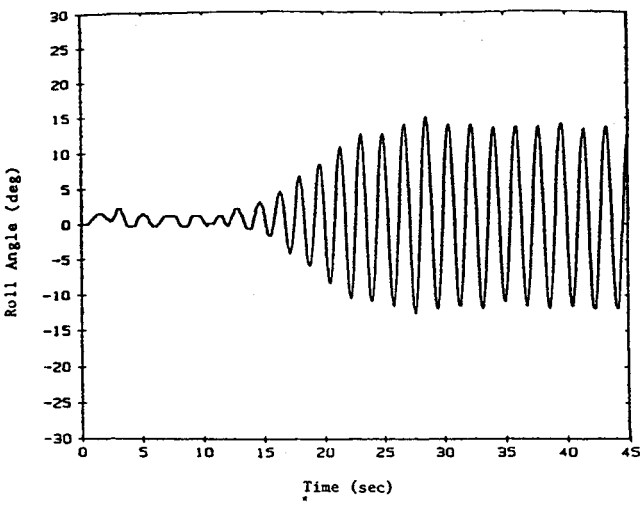

Fig. 14 Wing rock amplitude time history of subscale F-18 HARV model.[10] Angle of attack (deg) = 40 and $Re = 24.9 \times 10^3$.

teristics shown in Fig. 8 or 13. Flow visualization of the wing rock[10] shows that the interaction between forebody and LEX vortices suddenly undergoes a dramatic change, the forebody vortex dipping down to interact strongly with the LEX vortex. That started the wing rock, with the forebody-LEX vortex interaction alternating between the two sides. The interaction between forebody and LEX vortices is likely to lift up the LEX vortex and promote the breakdown of both vortices. As a result, much of the beneficial effect of the LEX vortex, i.e., the delay of flow separation on the main wing due to the vortex-induced flowfield, is lost.

These flow visualization results[10] suggest the scenario for the F-18 wing rock[8] shown in Fig. 15. The downstream moving wall effect will delay flow separation for laminar flow conditions. In Fig. 15 the aerodynamic spring needed for the oscillatory wing rock motion is provided by the rolling moment generated by the loss of lift occurring on the main wing when the forebody vortex interacts with the LEX vortex.[8] As in the case of the generic aircraft model in Fig. 7, there is a

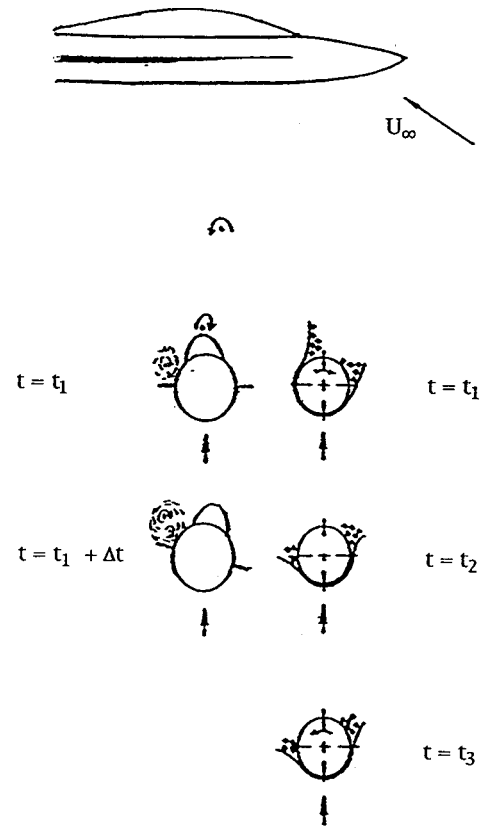

Fig. 15 Conceptual flow mechanism of the F-18 wing rock.[8]

time lag involved. After the separation asymmetry on the forebody has changed, it takes a finite time increment Δt before the strong interaction between forebody and LEX vortices has been completed. This generates the rolling moment that drives the wing rock motion.[8]

Conclusions

A review of available experimental results shows that wing rock of advanced aircraft will be driven by the vortices generated by forebody flow separation at high angles of attack, $\alpha > 30$ deg. The key flow phenomenon driving the forebody-induced wing rock is the coupling between forebody crossflow separation and vehicle motion. More precisely, the rolling motion generates moving wall effects that control the crossflow separation on the forebody and the associated vortices, thereby providing the feedback mechanism responsible for the observed wing rock. The limit cycle oscillation results when this driving rolling moment generated by the forebody vortices is balanced by the roll damping generated by the stalling wing.

Acknowledgments

The article is based upon work supported by ARPA under Contract DAAH01-92-R230; with Michael Francis as Technical Monitor. The authors are grateful to M. Francis for his support and helpful discussions throughout the course of this work. Figure 1b was shown in the oral presentation of Paper 94-0167. It is shown here by courtesy of the authors of AIAA Paper 87-2559.

References

[1]Ericsson, L. E., "Various Sources of Wing Rock," *Journal of Aircraft*, Vol. 27, No. 6, 1990, pp. 488–494.

[2]Ericsson, L. E. and Reding, J. P., "Fluid Dynamics of Dynamic Stall, Part I, Unsteady Flow Concepts," *Journal of Fluids and Structures*, Vol. 2, Jan. 1988, pp. 1–33.

[3]Brandon, J. M., and Nguyen, L. T., "Experimental Study of Effects of Forebody Geometry on High Angle of Attack Stability," *Journal of Aircraft*, Vol. 25, No. 7, 1988, pp. 591–597.
[4]Ericsson, L. E., "Wing Rock Generated by Forebody Vortices," *Journal of Aircraft*, Vol. 26, No. 2, 1989, pp. 110–116.
[5]Ericsson, L. E., "Further Analysis of Wing Rock Generated by Forebody Vortices," *Journal of Aircraft*, Vol. 26, No. 12, 1989, pp. 1098–1104.
[6]Fratello, D. J., Croom, M. A., Nguyen, L. T., and Domack, C. S., "Use of the Updated NASA Langley Radio-Controlled Drop-Model Technique for High-Alpha Studies of the X-29A Configuration," AIAA Paper 87-2559, Aug. 1987.
[7]Ericsson, L. E., "Prediction of High-Alpha Vehicle Dynamics," International Council of the Aeronautical Sciences, ICAS-90-3.5.1, Sept. 1990.
[8]Ericsson, L. E., "Separated Flow Mechanisms in F-18 Wing Rock," *Journal of Aircraft*, Vol. 33, No. 1, 1996, pp. 81–86.
[9]Klein, V., and Noderer, K. D., "Aerodynamic Parameters of the X-31 Drop Model Estimated from Flight Data at High Angles of Attack," AIAA Paper 92-4357, Sept. 1992.
[10]Quest, T., Nelson, R. C., and Fisher, D. F., "A Study of High-Alpha Dynamics and Flow Visualization for a 2.5% Model of the F-18 HARV Undergoing Wing Rock," AIAA Paper 91-3267, Sept. 1991.
[11]Ng, T. T., Ong, L. Y., Suarez, C. J., and Malcolm, G. N., "Wing Rock Suppression Using Forebody Vortex Control," AIAA Paper 91-3227, Sept. 1991.
[12]Ericsson, L. E., "Slender Wing Rock Revisited," *Journal of Aircraft*, Vol. 30, No. 3, 1993, pp. 352–356.
[13]Ng, T. T., private communication, Sept. 1991.
[14]Ericsson, L. E., and Reding, J. P., "Asymmetric Flow Separation and Vortex Shedding on Bodies of Revolution," *Tactical Missile Aerodynamics: General Topics*, edited by M. J. Hemsch, Progress in Astronautics and Aeronautics, AIAA, Washington, DC, 1992, pp. 391–452.
[15]Ericsson, L. E., "Moving Wall Effects in Unsteady Flow," *Journal of Aircraft*, Vol. 25, No. 11, 1988, pp. 977–990.
[16]Swanson, W. M., "The Magnus Effect: A Summary of Investigations to Date," *Journal of Basic Engineering*, Vol. 83, Sept. 1961, pp. 461–470.
[17]Mendenhall, M. R., Perkins, S. C., and Ericsson, L. E., "Prediction of Forebody Vortex-Induced Wing Rock," AIAA Paper 93-3451, Aug. 1993.
[18]Achenbach, E., "Influence of Surface Roughness on the Cross-Flow Around a Circular Cylinder," *Journal of Fluid Mechanics*, Vol. 46, Pt. 2, 1971, pp. 321–335.
[19]Mendenhall, M. R., Perkins, S. C., Jr., and Leisiutre, D. J., "Vortex Cloud Model for Body Vortices and Tracking," *Tactical Missile Aerodynamics: Prediction Methodology*, edited by M. R. Mendenhall, Vol. 142, Progress in Astronautics and Aeronautics, AIAA, Washington, DC, 1992, pp. 225–285.
[20]Nguyen, L. T., Whipple, R. D., and Brandon, J. M., "Recent Experiences of Unsteady Aerodynamic Effects on Aircraft Flight Dynamics at High Angle of Attack," AGARD CP-386, Nov. 1985.
[21]Brandon, J. M., Murri, D. C., and Nguyen, L. T., "Experimental Study of Effects of Forebody Geometry on High Angle of Attack Static and Dynamic Stability and Control," International Council of the Aeronautical Sciences, ICAS Paper 86-5.4.1, Sept. 1986.

IMPORTANT ANNOUNCEMENT

New Editor-in-Chief Sought for the *AIAA Journal*

George W. Sutton, current Editor-in-Chief of the *AIAA Journal*, will relinquish his position at the end of 1996. We are seeking an outstanding candidate with an international reputation for this position, and we invite your nominations.

The Editor-in-Chief is responsible for maintaining the quality and reputation of the journal. He or she receives manuscripts, assigns them to Associate Editors for review and evaluation, and monitors the performance of the Associate Editors to assure that the manuscripts are processed in a fair and timely manner. The Editor-in-Chief works closely with AIAA Headquarters staff on both general procedures and the scheduling of specific issues. Detailed record keeping and prompt actions are required. The Editor-in-Chief is expected to provide his or her own clerical support, although this may be partially offset by a small expense allowance. AIAA provides a computer, together with appropriate manuscript-tracking software.

Interested candidates are invited to send full résumés, including a complete list of published papers, to:

Norma Brennan
American Institute of Aeronautics and Astronautics
1801 Alexander Bell Drive, Suite 500
Reston, VA 22091
Fax 703/264-7551

Two letters of recommendation also are required. The recommendations should be sent by the parties writing the letters directly to Ms. Brennan at the above address or fax number. All materials must be received at AIAA Headquarters by **May 31, 1996**.

A selection committee will review the applications and will recommend qualified candidates to the AIAA Vice President–Publications, who in turn will present a recommendation to the AIAA Board of Directors for approval. All candidates will be notified of the final decision.

AIAA